



## NUMERICAL SIMULATION OF FLUID-STRUCTURE COUPLED PROBLEMS

<sup>1</sup>prof. dr.sc. **Jure Radnić**

<sup>1</sup>prof. dr. sc. **Alen Harapin**

<sup>1</sup>prof. dr.sc **Domagoj Matešan**

<sup>1</sup>**Nikola Grgić**

<sup>1</sup>**Marija Smilović**

<sup>1</sup>**Marina Sunara**

<sup>1</sup>Arhitektonsko-građevinski fakultet u Splitu Sveučilište u Splitu

<sup>2</sup>mr.sc.**Goran Šunjić**

<sup>2</sup>**Ante Džolan**, mag.građ.

<sup>2</sup>Građevinski fakultet Sveučilišta u Mostaru

**Summary:** This paper briefly describes the numerical models for the simulation of fluid-structure coupled problems. The applied models are primarily intended to simulate the fluid-structure dynamic interaction in seismic conditions. Models can simulate the most important non-linear effects of plane and spatial structures that are in direct contact with fluid. Some of models' possibilities are illustrated in numerical analyses of the seismic behavior for several practical examples.

**Keywords:** Numerical model, coupled problems, fluid-structure interaction, seismic behavior

## NUMERIČKA SIMULACIJA VEZANIH PROBLEMA FLUID-KONSTRUKCIJA

**Rezime:** U radu su ukratko prikazani numerički modeli za simulaciju tzv. vezanog problema interakcije fluida i konstrukcije. Primijenjeni modeli su prvenstveno namenjeni za simulaciju interakcije fluida i konstrukcije u seizmičkim uvjetima. Modelima se može da simuliraju najznačajniji nelinearni efekti ravanskih i prostornih konstrukcija koje su u direktnom doticaju s tečnošću. Neke moguće modele prikazane su kroz numeričku analizu nekoliko praktičnih građevina pod seizmičkim delovanjem.

**Ključne reči:** numerički model, vezani problem, interakcija fluid-konstrukcija, seizmičko delovanje

Rad objavljen: International Conference marking 60 years of operation of DIMK Serbia - Research in the field of building materials and structures, Proceedings, page 167, Belgrade, Republic of Serbia. 19 October 2012.



## 1. INTRODUCTION

Department of Concrete Structures and Bridges at the University of Split, Faculty of Civil Engineering, Architecture and Geodesy, has already more than 25 years in research and developing of models and software for analysis of structures which are in direct contact with fluid. In the last 10 years the researchers from Faculty of Civil Engineering University of Mostar joined with them in improvement the old and development of new techniques and models for this problem.

During past years the developed software was tested on various examples from literature. Also, these researches were basis for many articles which were published in journals and conference proceedings, as well as books chapters. Also, developed software was used as useful tool for design and calculation of many standard engineering structures of practical proposes.

Structures which are in direct contact with fluid, for example: dams, water tanks (reservoirs), off shore structures, pipelines and water towers etc, can often be encountered in engineering practice. Numerical models for real simulations of these structures have to include the simulation of the fluid-structure interaction to ascertain the real behavior of this complex system. This problem is particularly emphasized under dynamic/seismic conditions and it is commonly referred to as a coupled (multi-field) problem [3, 30].

Some of those structures can be seen on Fig. 1.



Figure 1. Examples of structures in direct contact with fluid

A coupled multi field problem involves two or more interacting fields, for example: gravity dam with accumulation, water tower full of water etc. Such a problem is time dependent and the state of one field is continuously linked to the state of other fields and neither field can be solved independently from the other. Here, the coupling normally occurs through the differential equation representing different physical phenomena. The coupled fields may be overlapping as in case of seepage and thermo-mechanical problems. On the other hand, the coupled fields may be non-overlapping as in fluid-structure interaction problems as discussed in this work. Here, the coupling occurs due to the imposed boundary condition at the interface. The fields may be coupled with all the other participating fields or with only few of them. The coupling in some problems like seepage may disappear when steady state is reached [3].

Two main approaches exist for the simulation of fluid. structure interaction problems:

- Monolithic approach: the equations governing the fluids pressures and the displacement of the structure are solved simultaneously, with a single solver
- Partitioned approach: the equations governing the fluids pressures and the displacement of the structure are solved separately, with two distinct solvers



The monolithic approach requires a code developed for particular combination of physical problems whereas the partitioned approach preserves software modularity because an existing fluid solver and structural solver are coupled. Moreover, the partitioned approach facilitates solution of the fluid equations and the structural equations with different, possibly more efficient techniques which have been developed specifically for either fluid equations or structural equations.

Thus the partitioned approach has various advantages: (i) the resulting model is very modular, (ii) it's easy to make any modifications, (iii) every modification in one field improves the whole model, (iv) the programmer/improver can have knowledge in (only) a single field.

This article briefly describes the developed models and software for numerical modeling of the dynamic interaction of water-structure systems. The described models are suitable for problems with limited fluid motions, such as the response of offshore structures and dams to waves or earthquake.

## 2. NUMERICAL MODELS

### 2.1. Introduction

All solutions shown here are based, as it mentioned earlier, on the partitioned scheme where individual fields are solved independently by considering the interaction information transfer between them at every stage of the solution process. This approach allows the usage of ordinary approaches and appropriate mathematical/physical models for separate fields (structure and fluid) that include minor modifications for the influence of interactions.

Developed models and software are based on finite elements method for the spatial discretization and finite differences method for the time discretization of the system [1-3]. For structure and soil the displacement formulation is used, and for fluid the displacement potential formulation is used [3, 30].

In articles [1-5] the basic algorithms for separate fields as well as for fluid-structure interaction problems are given. Furthermore, articles [6-7] present the development of non-linear numerical models for dynamic interactions of the fluid-soil-structure system for plane and spatial problems.

Some non-linear models for structures are described in articles [8-13], and some models for solve eigen value problem are presented in articles [14, 15].

Articles [16-21] present some recent works in this field.

### 2.2. Numerical model for fluid

#### 2.2.1. Introduction

A fluid is a substance (either a liquid or a gas) that continuously deforms under the action of applied surface stresses. Fluid flow may be classified as either inviscid or viscous. Inviscid flows are frictionless flows characterized by zero viscosity. No real flows are inviscid, but there are numerous fluids and flow situations in which viscous effects can be neglected. Often viscosity effects are confined to thin regions or boundary layers near flow boundaries, and the rest of the flow can be considered frictionless. Inviscid flows may be further classified as either compressible or incompressible, depending on whether density variations are large or relatively unimportant. In this investigation the fluid is considered inviscid and the Eulerian formulation is used [3].



### 2.2.2. Displacement Potential Formulation

The behavior of fluid, in the most general form, can be expressed by Navier-Stokes equations:

$$\frac{\partial v_i}{\partial t} = R_i - \nabla p + \nabla^2 v_i \quad (1)$$

In this equation  $\rho$  represent the density of the fluid,  $v_i$  the fluid velocity,  $p$  the pressure,  $R_i$  the gravitational forces and  $\mu$  is the dynamic viscosity.

The displacement potential is defined as:

$$\nabla \cdot \mathbf{u} = -\nabla^2 \phi \quad (2)$$

The  $u_i$  are the displacements, which can be expressed:

$$u_i = \frac{\partial \phi}{\partial x_i} = \nabla \phi = -\frac{p}{E} \quad (3)$$

where  $E$  represent the bulk modulus.

If the changes in fluid density ( $\rho$ ) can be neglected, then using (2), Navier-Stokes equations (1) can be reduced, and with neglecting of viscosity and gravitational forces, the equation (1) becomes:

$$\nabla^2 \phi = \nabla p \quad (4)$$

This formulation is called displacement potential formulation, and is in very common use, because it can easily described non-linear fluid behavior, which will be shown later.

Spatial integration of (4) yields:

$$\phi = p \quad (5)$$

and by eliminating  $p$ ,  $u$  and  $\rho_f$  from (3), (4) and (5) we obtain:

$$\nabla^2 \phi = \frac{1}{c^2} \frac{\partial^2 \phi}{\partial t^2} \quad (6)$$

where  $c$  is sound velocity in fluid. The equation (6) represents well known wave equation for inviscid fluid.

### 2.2.3. Boundary conditions

(i) The prescribed pressure on the free surface may be expressed as:

$$p = \rho_f g \frac{\partial \phi}{\partial n} \quad (7)$$

(ii) On moving boundaries, where  $u_n$  is the normal displacement of the surface:

$$\frac{\partial \phi}{\partial n} = -u_n \quad (8)$$

On a rigid boundary  $u_n=0$ , therefore,  $\frac{\partial \phi}{\partial n}=0$ . In the case of a base excitation,  $u_n$  is composed of the translation at the base and the relative displacement of the structure with respect to the base.



(iii) At radiating boundaries (Sommerfeld's condition):

$$\partial \Psi / \partial n = - \dot{\Psi} / c \quad (9)$$

#### 2.2.4. Finite element discretization

Using the standard finite element Galerkin process:

$$\begin{aligned} \Psi &= \mathbf{N}_\Psi \Psi \\ \mathbf{u} &= \mathbf{N}_u \bar{\mathbf{u}} \end{aligned} \quad (10)$$

where  $\mathbf{N}_\Psi$  and  $\mathbf{N}_u$  are the shape functions for displacement potential  $\Psi$  and structural boundary displacement  $\mathbf{u}$ , then it can be shown that:

$$\mathbf{M}_f \ddot{\Psi} + \mathbf{C}_f \dot{\Psi} + \mathbf{K}_f \Psi = \mathbf{f}_f - \mathbf{Q}_t(\mathbf{u} + \mathbf{d}) \quad (11)$$

Above equation represent the differential equation of dynamic equilibrium of system, in matrix formulation. In equation (11),  $\mathbf{M}_f$  is the mass matrix of the fluid;  $\mathbf{C}_f$  is the radiation damping matrix;  $\mathbf{K}_f$  is the stiffness matrix of the fluid;  $\mathbf{f}_f$  is the vector of applied nodal forces;  $\mathbf{Q}_t$  is the fluid-structure interaction matrix;  $\Psi$  is the vector of unknown displacement potential;  $\rho_f$  is the density of the fluid;  $\mathbf{u}$  is vector of displacements of the moving boundary relative to the base and  $\mathbf{d}$  is the vector of base excitations.

Above matrices can be expressed:

$$\begin{aligned} (\mathbf{K}_f)_{ij} &= \int_{V_f} \left[ \left( \frac{\partial \mathbf{N}_{\Psi i}}{\partial x} \frac{\partial \mathbf{N}_{\Psi j}}{\partial x} \right) + \left( \frac{\partial \mathbf{N}_{\Psi i}}{\partial y} \frac{\partial \mathbf{N}_{\Psi j}}{\partial y} \right) + \left( \frac{\partial \mathbf{N}_{\Psi i}}{\partial z} \frac{\partial \mathbf{N}_{\Psi j}}{\partial z} \right) \right] dV \\ (\mathbf{C}_f)_{ij} &= (1/c) \int_{\Omega_r} \mathbf{N}_{\Psi i}^T \mathbf{N}_{\Psi j} d\Omega \\ (\mathbf{M}_f)_{ij} &= (1/g) \int_{\Omega_f} \mathbf{N}_{\Psi i}^T \mathbf{N}_{\Psi j} d\Omega + (1/c^2) \int_{V_f} \mathbf{N}_{\Psi i}^T \mathbf{N}_{\Psi j} dV \\ (\mathbf{Q}_t)_{ij} &= \int_{\Omega_i} \mathbf{N}_{\Psi i}^T \bar{\mathbf{n}} \mathbf{N}_{\Psi j} d\Omega \end{aligned} \quad (12)$$

where  $V_f$  is the fluid domain;  $\Omega_r$  is the radiating fluid boundary;  $\Omega_f$  is the free surface boundary;  $\Omega_i$  is the interaction boundary. The solution procedure for (8) is described in Section 2.5.

#### 2.2.5. Nonlinear fluid model

In the fluid-structure interaction, nonlinearities are often confined to the structural behavior where the fluid is considered linear. Linear approach - pressure formulation, which presumes unlimited negative pressures in fluid, is natural and very suitable for this approach. However, the displacement potential formulation is more general, and can be used in linear or non-linear models.

The fluid can take some tension which depends upon the concentration and size of micro bubbles present in the fluid. However, if the absolute pressure in a subregion of fluid drops to a value close to vapor pressure of the fluid, bubbles are formed and this physical phenomenon is known as cavitation. Physically, cavitation occurs when the total absolute pressure is less than the vapor pressure of the fluid. Cavitation can cause significant damaging effects on solid surfaces.



Cavitation occur when the total absolute pressure is less then the vapor pressure of the fluid i.e.:

$$p_{abs} = p + p_h + p_a \leq p_v \tag{13}$$

where  $p_{abs}$  is the total absolute pressure,  $p$  is hydrodynamic pressure,  $p_h$  is hydrostatic pressure,  $p_a$  is atmospheric pressure and  $p_v$  is vapor pressure. This implies that cavitation occurs when the hydrodynamic pressure drops below  $(p_v - p_s)$ . The vapor pressure of water, for all practical purposes, can be taken from 0.02 to 0.03 MPa.

The changes which the fluid may undergo under hydrodynamic excitation are a direct function of the mass dilatation  $s$ , defined as:

$$s = \nabla^T (\rho_f \mathbf{u}_f) = \text{Div}(\rho_f \mathbf{u}_f) \tag{14}$$

where  $\mathbf{u}_f$  is displacement of the fluid relative to the initial static state. As long as  $p_{abs}$  is greater then the vapor pressure  $p_v$ , a linear relation between  $s$  and  $p$  is assumed:

$$p = -\alpha s \quad ; \quad \alpha = c^2 \tag{15}$$

where  $c$  is the acoustic velocity of the fluid.

If equation 13 is true, cavitation occurs and the stage of linear fluid is no longer valid. A simple fluid model can be represented by the bilinear pressure-mass dilatation relation shown in Fig. 2. Cavitation, therefore, commences when the following condition is reached:

$$s \geq (p_h + p_a - p_v) / c^2 \tag{16}$$

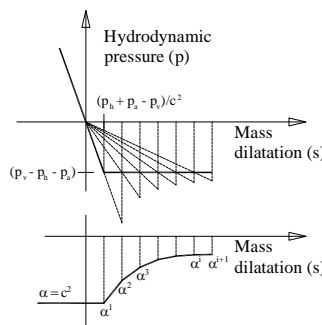


Figure 2. Relation between mass dilatation and hydrodynamic pressure

If cavitation occurs, the iteration procedure, shown in Fig. 2, has to be performed to obtain the value of the coefficient  $\alpha$ .

## 2.3. Numerical model for structure

### 2.3.1. Introduction

For dynamic equilibrium of a solid body in motion the Principle of virtual work can be used to write the equations independent of the material behavior:

$$\int_{\Omega} (\delta \underline{\underline{\varepsilon}})^T \underline{\underline{\sigma}} d\Omega - \int_{\Omega} (\delta \underline{\underline{u}})^T (b - \rho_s \underline{\underline{u}} - \mu' \underline{\underline{u}}) d\Omega - \int_{\Gamma_t} (\delta \underline{\underline{u}})^T t d\Gamma = 0 \tag{17}$$

where  $\delta \underline{\underline{u}}$  is the vector of virtual displacements,  $\delta \underline{\underline{\varepsilon}}$  is the vector of associated virtual strains,  $b$  is the vector of applied body forces,  $t$  is the vector of surface tractions,  $\underline{\underline{\sigma}}$  is the vector of



stresses,  $\rho_s$  is the mass density,  $\mu'$  is the damping parameter and a dot refers to differentiation with respect to time. The domain of interest  $\Omega$  has two boundaries:  $\Gamma_t$  on which boundary tractions  $\mathbf{t}$  are specified and  $\Gamma_u$  on which displacements are specified.

In dynamic analysis, the finite element method can be applied in both analyses: for space and time. However, it is the general practice to use finite elements in space and finite differences in time [1, 2, 3]. This approach is adopted in this work. Here, the displacement formulation is used because of its simplicity, generality and good numerical properties. For a finite element representation, the displacements and strains and also their virtual counterparts are given by the following relationships:

$$\begin{aligned}\underline{\mathbf{u}} &= \mathbf{N} \mathbf{u} & \delta \underline{\mathbf{u}} &= \mathbf{N} \delta \mathbf{u} \\ \underline{\boldsymbol{\varepsilon}} &= \mathbf{B} \mathbf{u} & \delta \underline{\boldsymbol{\varepsilon}} &= \mathbf{B} \delta \mathbf{u} \\ \underline{\boldsymbol{\sigma}} &= \mathbf{D} \underline{\boldsymbol{\varepsilon}} = \mathbf{D} \mathbf{B} \mathbf{u} & \delta \underline{\boldsymbol{\sigma}} &= \mathbf{D} \delta \underline{\boldsymbol{\varepsilon}} = \mathbf{D} \mathbf{B} \delta \mathbf{u}\end{aligned}\quad (18)$$

where  $\mathbf{u}$  is the vector of nodal displacements,  $\delta \mathbf{u}$  is the vector of virtual nodal variables,  $\mathbf{N}$  is the matrix of global shape functions,  $\mathbf{B}$  is the global strain-displacement matrix and  $\mathbf{D}$  is the global constitutive matrix.

If (18) are substituted into (17), and if we note that the resulting equation is true for any set of virtual displacements, then the following equation can be obtained:

$$\mathbf{M}_s \ddot{\mathbf{u}}_i + \mathbf{C}_s \dot{\mathbf{u}}_i + \mathbf{R}_s(\mathbf{u}_i) = \mathbf{f}_s \quad (19)$$

where:

$$\begin{aligned}(\mathbf{M}_s)_{kj} &= \int_{\Omega_s} \mathbf{N}_{sk}^T \rho_s \mathbf{N}_{sj} d\Omega \\ (\mathbf{C}_s)_{kj} &= \int_{\Omega_s} \mathbf{N}_{sk}^T \mu' \mathbf{N}_{sj} d\Omega \\ \mathbf{R}_s(\mathbf{u}_i) &= \int_{\Omega_s} \mathbf{B}^T(\mathbf{u}_i) \boldsymbol{\sigma}_i d\Omega \\ (\mathbf{f}_s)_i &= \int_{\Omega_s} \mathbf{N}_{sk}^T \mathbf{b}_i d\Omega + \int_{\Gamma_t} \mathbf{N}_{sk}^T \mathbf{t}_i d\Gamma\end{aligned}\quad (20)$$

where  $\mathbf{N}$  is the matrix of global shape functions.

For real structures, relationship strain-deformation is generally non-linear:

$$\boldsymbol{\varepsilon} = \mathbf{B} \mathbf{u} \quad ; \quad \mathbf{B} = \mathbf{B}(\mathbf{u}) \quad (21)$$

which represent so called geometrical nonlinearity. In fact, because of geometry transformation, array  $\mathbf{B}$  is not linear but depends on system displacement. Relationship  $\boldsymbol{\varepsilon}$ - $\mathbf{u}$  is known as model of geometry.

Relationship between stress ( $\boldsymbol{\sigma}$ ) and strain ( $\boldsymbol{\varepsilon}$ ) is also generally nonlinear, and represent material nonlinearity. It is usually called material model or constitutive relationship.

In all calculation, origin point is linear elastic behavior. For example, for a plane strain state and isotropic elastic material, matrix  $\mathbf{D}$  is given as:

$$\mathbf{D} = \frac{E}{(1+\nu)(1-2\nu)} \begin{bmatrix} (1-\nu) & \nu & 0 \\ \nu & (1-\nu) & 0 \\ 0 & 0 & \frac{(1-2\nu)}{2} \end{bmatrix} \quad (22)$$



where  $E$  and  $\nu$  is well known Young's elasticity modulus and Poisson's ratio, respectively.

### 2.3.2. Structure nonlinearity

Two main types of nonlinearity which occur in structures are the geometrical and the material nonlinearity, as mentioned earlier.

#### Geometric nonlinearity

Structures may undergo either (i) small deformations which are negligible compared to the dimensions of the body or (ii) large or finite deformations in which the theory of small deformations is no longer valid. The second type of deformation is termed geometrically nonlinear problems and special procedure is required for their solutions. In many real civil engineering structures geometric nonlinearity can be neglected.

#### Material nonlinearity

Deformations may be divided in recoverable or unrecoverable. A recoverable deformation implies that when the load is removed, the solid body retains its original position, whereas an unrecoverable deformation implies that when the load is removed, the solid body exhibit permanent deformations. All real materials have nonlinear behavior, but in many cases material can be consider linear.

Many types of material model were developed to represent the variety of behavior such as linear elastic, nonlinear elastic, elasto-plastic, visco-elastic, visco-plastic, creep, cracking or fracture etc. Different hardening laws such as isotropic and kinematic hardening also developed in the plastic and visco-plastic models. Apart from the linear elastic models, all of these representations are nonlinear in some sense.

### 2.3.3. Numerical model for reinforced concrete structures

A special material model was developed for the simulation of reinforced concrete structures [11-15, 22, 24]. It includes the most important nonlinear effects of reinforced concrete behavior: yielding in compression and opening and propagation of cracks in tension, with tensile and shear stiffness of cracked concrete, as well as nonlinear behavior of reinforced steel. In every integration point of every element, simulation of cracks opening and closing is possible.

Special materials models were developed for plane (2D) problems, spatial (3D) problems and for shell structures. These models will be only briefly discussed here, and for further reading can be found in quoted references.

#### Yielding in compression

There is still no accepted constitutive model which could describe the complexity of concrete behavior under different stress states. Various models have been proposed for describing the stress-strain relation under multiaxial static stresses. Each of these has certain advantages and disadvantages, considering the analyzed problem. The simplified models, based on small number of the basic concrete parameters, are better for engineering practice because complex models based on greater number of parameters, cannot be used.

A rather simple concrete model is preferred (Fig. 3), intended for ordinary engineering practice, founded on basic concrete parameters (uniaxial compressive and tensile strength, the modulus of elasticity and Poisson's ratio) which should be known for other purposes anyway.

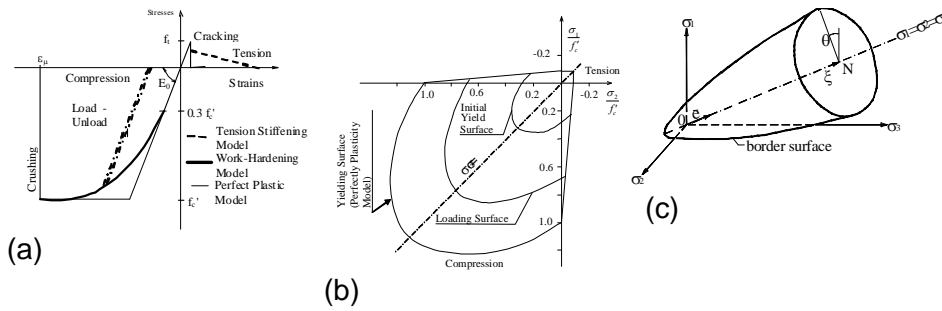


Figure 3. Non-linear behavior of concrete in compression (yielding) .  
1D (a), 2D (b) and 3D (c) problems

Modeling of cracks

The graphic interpretation of the concrete model under tension, for 2D problems, is presented in Fig. 4. Linear-elastic behavior has been assumed until tensile strength of concrete  $f_t$  is reached. After that, the first crack in concrete is assumed to appear perpendicular to main tensile stress.

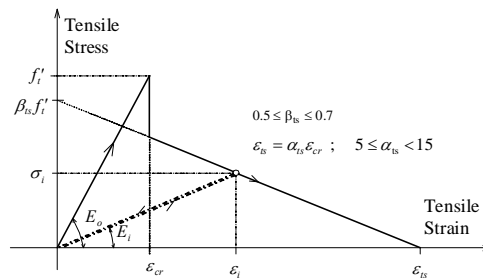


Figure 4. Graphical representation of concrete behavior in tension

It is also assumed that, even after cracking, the concrete remains as a continuum. A model of the so-called smeared cracks has been used. It has been adopted that after the occurrence of the first crack, its position and direction do not change after subsequent changes of loading. Hence, the so-called model of fixed orthogonal cracks has been used.

After the occurrence of cracks, concrete becomes anisotropic and the cracks directions define the main axis of anisotropy. Both, partial and complete crack closings at unloading have been modeled, as well as new opening of the previously developed cracks under repeated loading. The potential states of cracks, for 2D and 3D problems, are presented in Fig. 5.

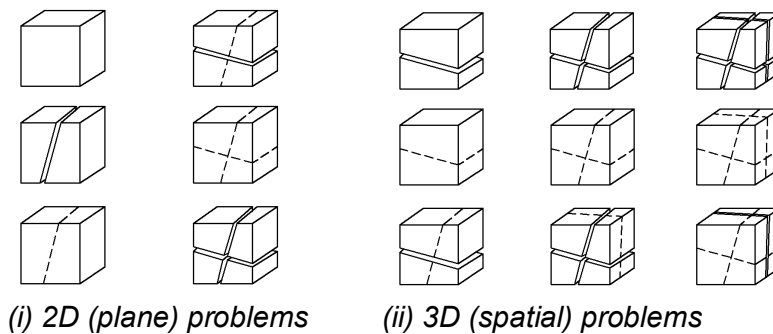


Figure 5. Schematic presentation of possible cracks pattern



The stiffness contribution of uncracked concrete between cracks was simulated by gradually decreasing the component of tensile stress perpendicular to the crack plane.

**Modeling of reinforcement**

The reinforcement model is graphically presented in Fig. 6, and the adopted stress-strain relationship for steel is presented in Fig. 7.

The reinforcement bars are modeled as separate beam elements incorporated in base elements (Fig. 6a and 6b). The stresses can occur only in the bars direction. It was assumed that the concrete and reinforcement displacements were entirely compatible. Detail description of this model can be found in [11, 24].

A bi-linear stress-strain relation was used to describe the steel behavior, both in compression and in tension. For unloading conditions, a linear behavior with the initial modulus of elasticity was assumed. The bars collapse occurs when the strain in their direction exceeds the limit value  $\epsilon_{su}$ .

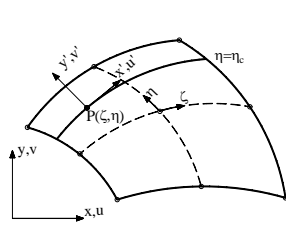


Figure 6a. Modeling of Reinforcement for 2D problems

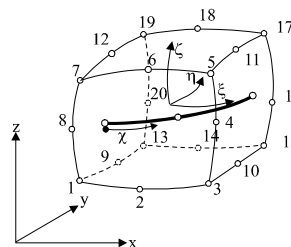


Figure 6b. Modeling of Reinforcement for 3D problems

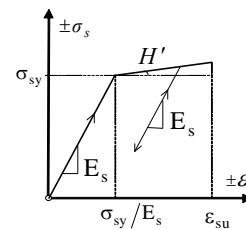


Figure 7. Stress-Strain Relation for Steel

**Model for composite joint**

Interface elements (Fig. 8) are used for simulation of continuous connection between two composite members [14, 15, 22]. They physically represents connection surface of base composite elements with determinate little width  $w$  (Fig. 9). These elements allow the simulation of sliding, splitting, detachment and impress on contact surface, according on acquired models of the interface element material behavior.

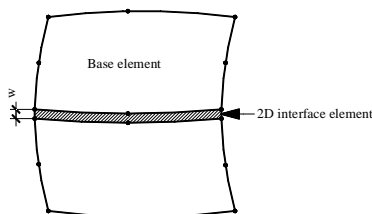


Figure 8. Interface element

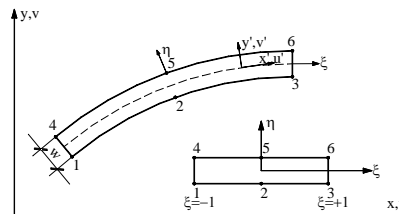


Figure 9. Interface element in global (x,y) and local (xi, eta) coordinate system



## 2.4. Equation for Coupled Fields Motions and Spatial Discretization

### 2.4.1. Coupled Fields Motions

Behavior of the fluid-structure system (structure includes the structure itself as well as the surrounding soil) in dynamic load conditions, can be expressed with two second order differential equations [1, 3, 5-7]. If we use the displacement formulation for the structure and the displacement potential formulation for the fluid, dynamic equilibrium equations can be expressed in the following form:

$$\begin{aligned} \mathbf{M}_s \ddot{\mathbf{u}} + \mathbf{C}_s \dot{\mathbf{u}} + \mathbf{K}_s \mathbf{u} &= \mathbf{f}_s - \mathbf{M}_s \ddot{\mathbf{d}} + \mathbf{f}_{cs} \\ \mathbf{M}_f \ddot{\Psi} + \mathbf{C}_f \dot{\Psi} + \mathbf{K}_f \Psi &= \mathbf{f}_f + \mathbf{f}_{cf} \end{aligned} \quad (23)$$

where

$$\begin{aligned} \mathbf{f}_{cs} &= \mathbf{Q} \Psi \\ \mathbf{f}_{cf} &= - \mathbf{Q}^T (\mathbf{u} + \mathbf{d}) \end{aligned} \quad (24)$$

In the above equations  $\mathbf{M}_s$ ,  $\mathbf{C}_s$  and  $\mathbf{K}_s$  represent mass, damping and stiffness matrices for structure, and  $\mathbf{M}_f$ ,  $\mathbf{C}_f$  and  $\mathbf{K}_f$  represent mass, damping and stiffness matrices for fluid. Vectors  $\mathbf{u}$ ,  $\dot{\mathbf{u}}$ ,  $\ddot{\mathbf{u}}$  represent structures displacements and displacements derivations (velocities and accelerations) and  $\Psi$ ,  $\dot{\Psi}$ ,  $\ddot{\Psi}$  are the displacement potential and associated derivations.  $\mathbf{Q}$  is the interaction matrix between structure and fluid.

Interaction between structure and base soil is modeled indirectly by contact elements in the connection surface. In fact, by applying the appropriate material model for contact elements, various effects in the contact surface can be simulated, such as: separating, embedment and sliding.

Fluid-structure interaction surface with fluid and structure elements is shown in Fig. 10. Interaction matrix  $\mathbf{Q}$  includes only the surface integration and is defined as:

$$(\mathbf{Q})_{ij} = \int_{\Gamma_i} \mathbf{N}_{ui}^T \bar{\mathbf{n}} \mathbf{N}_{pj} d_i \quad (25)$$

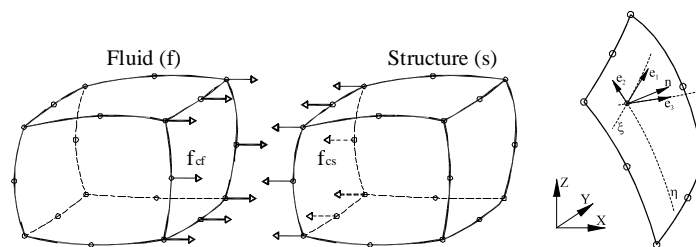


Figure 10. Fluid-structure interaction surface and unit norm

### 2.4.2. Spatial Discretization

As mentioned before, for plane (2D) problems, 8-node and 9-node isoparametric elements are used for fluid and structure. For spatial (3D) problems, 20-node and 27-node (brick) elements are used for fluid and structure. For thin curved structures, 8-node or 9-node degenerated shell elements can be used for structure and 20 or 27-node spatial



element for fluid. Those shell elements are free of membrane and shear locking, according to [10].

For the simulation of connections between the foundation soil and the structure, 6-node contact elements can be used for plane and 16 or 18 nodes for spatial problems.

Elements for 3D (spatial) problems are presented on Fig. 11, and elements for shell structures on Fig. 12.

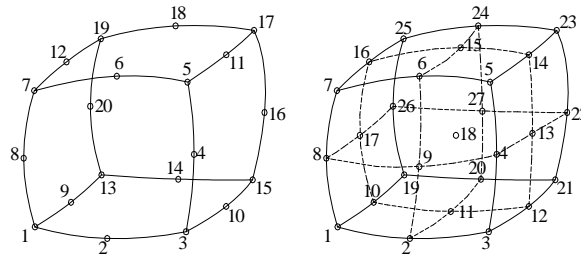


Figure 11. Elements for spatial (3D) discretization

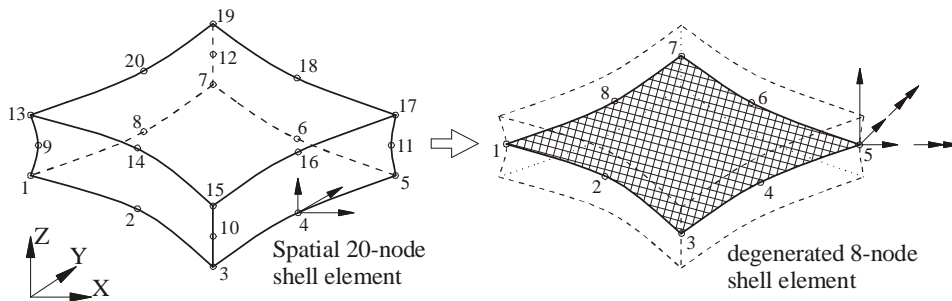


Figure 12. Elements for shell structures

## 2.5. Solution Concept for the Dynamic Fluid-Structure Interaction Problem

Direct solution of the equation system (23) requires large computer capacity. So, the previously described partitioned scheme is ideal for this kind of problems. In that approach for every increment of the imposed load and every non-linear problem iteration step, each field is solved separately by including interaction forces on the contact surface between fluid and structure. Presentation of the solution scheme is given in Fig. 13.

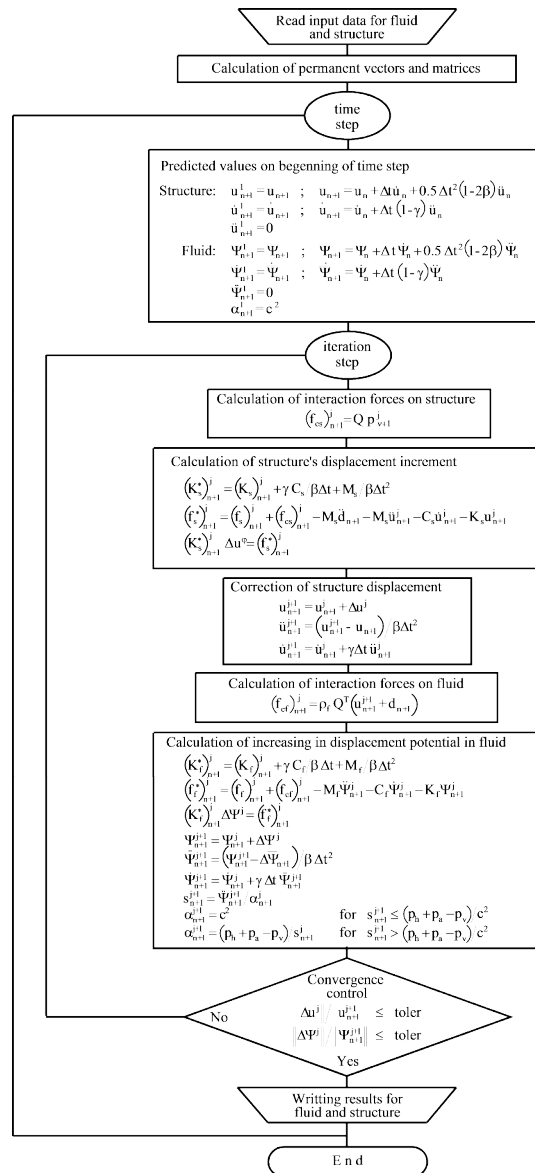


Figure 13. Flow chart for the solution of the fluid-structure coupled problem

In the presented approach, structure is solved first and fluid second. This approach allows the developed independent models to be used for each field (partition analysis), with additional calculations of the interaction forces only. Thus, in the fluid-structure interaction model, all non-linear effects of material and geometry, that are present in a particular field, can also be simulated in the coupled problem. In Fig. 13 for time integration, explicit-implicit algorithm developed by Hughes [1, 2] is used.

Predicted values  $u, \dot{u}, \ddot{u}$  and  $\psi, \dot{\psi}, \ddot{\psi}$  at the beginning of every time step are corrected at the end of the same time step. For convergence control of the iterative procedure, the increase of the structure's displacements in comparison with current total displacements and the increase of the fluid's displacements potential in comparison with the current total displacements potential are simultaneously monitored. Various options of the Newton-Raphson method are used to solve the non-linear equations.



## 2.6. Additional Model Possibilities

Solution of eigen value problem is also based on the partition solution scheme, with the Wilson-Yuan-Dickens (so-called WYD) method [4, 8, 9, 23] as the solution procedure. In dynamic problems, as well as in the structures response calculations, eigen values and eigen vectors are needed to know the vibration characteristics (determination of time step length).

Radiation damping can be simulated on artificially formed fluid boundaries, as well as radiation and multi-axis structure damping for structure [2, 5, 6].

Simulation of fluid pressure in open cracks of a structure is included by additional nodal forces in finite elements that have cracks that fluid can get into.

As external dynamic forces, various time-dependant dynamic loads can be applied. Also, seismic base excitations can be applied to the model.

Complex system structure-soil-fluid can be loaded with arbitrary seismic excitation in direction of three main axes, which can be given by series of measured (accelerograph) or generated input data in discrete time steps.

The computer programs (software) are equipped with adaptive and user-friendly postprocessor for the visualization of various numerical results.

## 3. EXAMPLES

What follows are four complex practical examples which illustrate some possibilities of the developed models and the applied software.

### 3.1. Example 1- Koyna Dam

The Koyna Dam is the largest dams in Maharashtra, India. It is a rubble-concrete dam constructed on Koyna River. It is located in Koyna Nagar, Satara district, nestled in the Western Ghats on the state highway between Chiplun and Karad. The dam, built in 1963, is one of the largest dams in India (Fig. 14). It is an atypical gravitational dam, with a crest length of 853.44 meters. It consists of 56 dilatation blocks of 17.07 m in thickness. Spillway length is 91.44 m.

Fig. 15 presents the main geometric data of the Koyna dam. Detailed information of the dam geometry, construction materials, damages (cracks) and earthquake characteristics can be found in [25, 26].

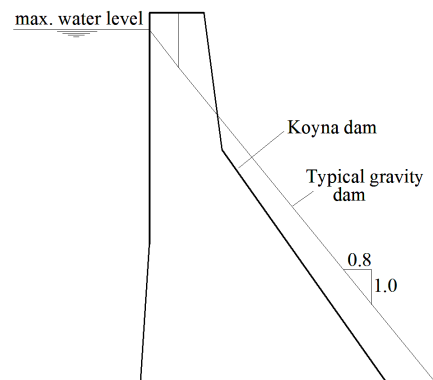


Figure 14. Koyna dam, photograph [33] and comparison with typical gravity dam [26]



During construction, two accelerographs were embedded in the dam, and in one of them, in 1967, an earthquake that caused several significant damages was registered. Dominant damages of the dam manifested as horizontal cracks on the up-stream and down-stream sides on many blocks, especially on lines where the total thickness of the dam changes.

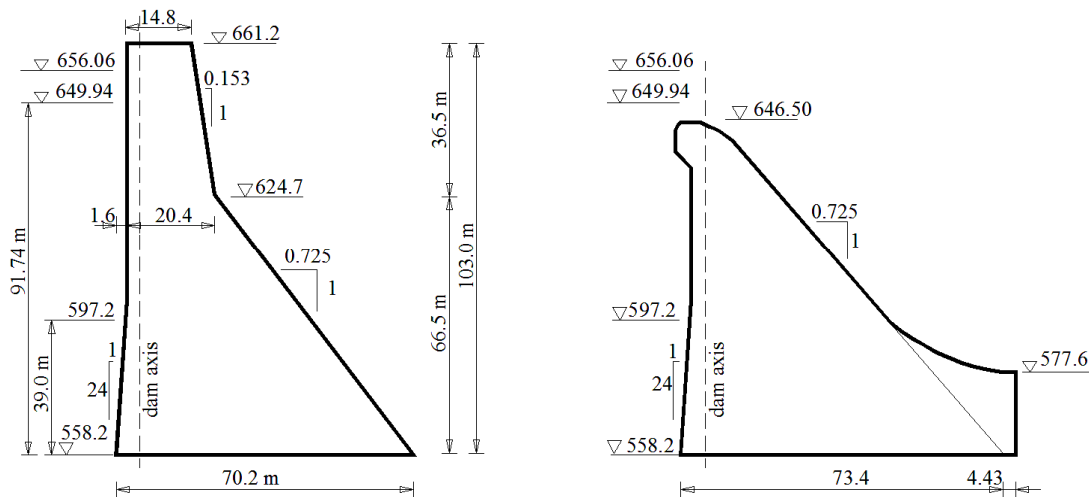


Figure 15. Koyna dam . some geometrical data (all dimensions are in meters) [26]:  
(a) cross-section through dam body; (b) cross-section through spillway

Spatial discretization of the system is presented in Fig. 16, and the used material characteristics are presented in Tab. 1. The behavior of the water-dam-soil system was analyzed for the previously mentioned registered earthquake. The system was analyzed separately for the linear and for the non-linear (cavitation) fluid model, with the following structure models: a) non-linear model without including the fluid pressure in open structure cracks (no FPC), b) non-linear model which includes the fluid pressure in open structure cracks (FPC).

Some numerical results are presented in Figs. 17 and 18. Other results can be found in [25, 26]. Dam damages calculated through numerical models match the real crack pattern very well.

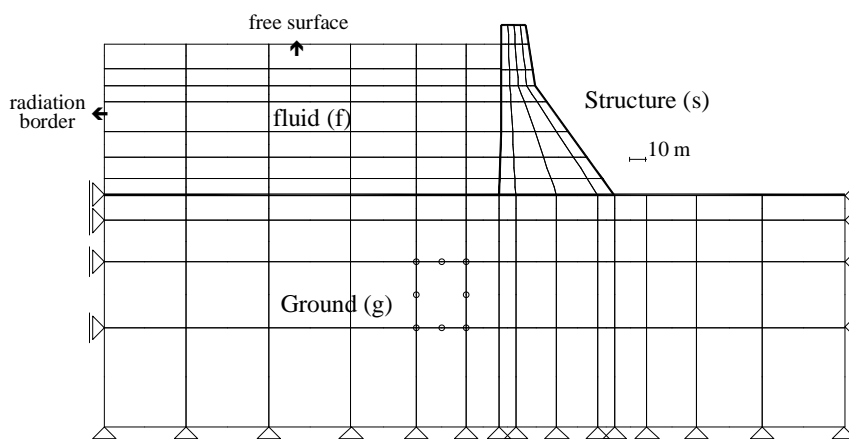


Figure 16. Spatial discretization of Koyna dam



Fluid (water)	Structure (concrete dam)	Ground
$\rho_f = 1019.0 \text{ kg/m}^3$ $c = 1439.0 \text{ m/s}$ $p_a = 0.10 \text{ MPa}$ $p_v = 0$	$E_s = 31640.0 \text{ MPa}$ $\nu_s = 0.2$ $\rho_s = 2690.0 \text{ kg/m}^3$ $(f'_c)_s = 24.6 \text{ MPa}$ $(f'_t)_s = 2.46 \text{ MPa}$ $(\epsilon_{cu})_s = 0.003$ $(\max \epsilon_t)_s = (\max \epsilon_{sh})_s = 0.0012$	$E_g = 18000.0 \text{ MPa}$ $\nu_g = 0.2$ $\rho_g = 1830.0 \text{ kg/m}^3$ $(f'_c)_g = 20.0 \text{ MPa}$ ; $(f'_t)_g = 2.0 \text{ MPa}$ $(\epsilon_{cu})_g = 0.003$ ; $(\max \epsilon_t)_g = (\max \epsilon_{sh})_g = 0.0017$

Table 1. Material characteristics of the Koyna dam system

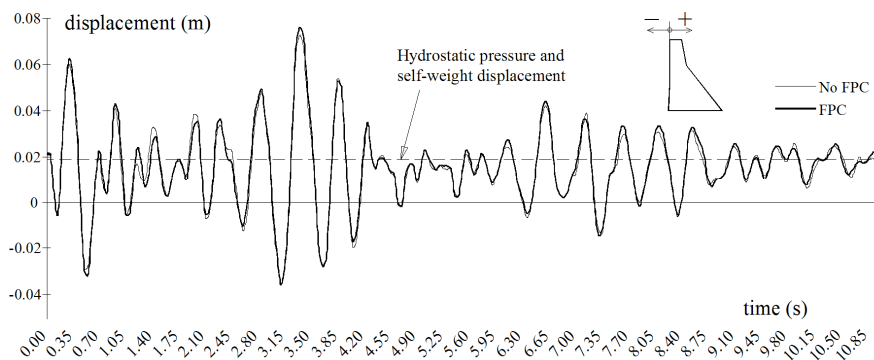


Figure 17. Horizontal displacement of the Koyna dam crest for non-linear fluid model

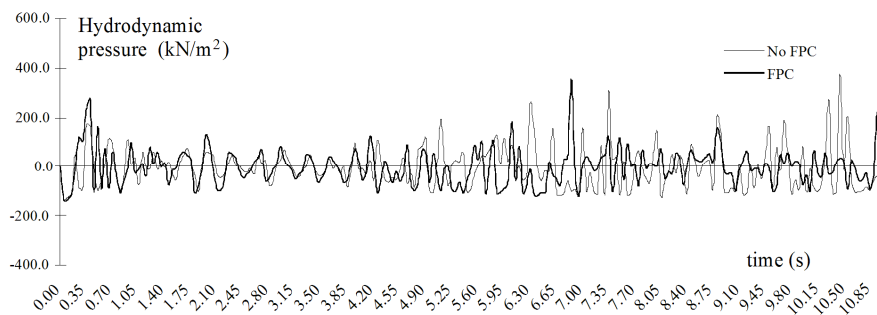


Figure 18. Hydrodynamic pressure at the bottom of the Koyna dam

### 3.2. Example 2- Grančarevo Dam

The Gran arevo Arch Dam in Bosnia and Herzegovina (Figs. 19, 20, 22) is a double-curvature concrete dam with a perimetral joint. The dam was constructed in 1968. The height of the dam is 123 meters and the crest length is 439 meters. Its bottom thickness is 27 meters and its top thickness 4.6 meters. The dam's foundation dig was 230.000 m<sup>3</sup> and the volume of poured concrete was 376.000 m<sup>3</sup>. The head of the dam is 100 meters. The dam created the Bile a reservoir with a maximum water depth of 51 meters and an available storage capacity of 1100 million cubic meters. The Bile a reservoir is the largest storage lake in Balkan. Its dimensions are: total storage volume: 1280 hm<sup>3</sup> and surface of the reservoir on normal top water level: 2764 ha. Geometrical data tables (on Fig. 21) show basic geometrical



characteristics for individual arches some of which are shown in Fig. 20 and 21. Other detailed information about dam can be found in [27-31].



Figure 19. Gran arevo Arch Dam

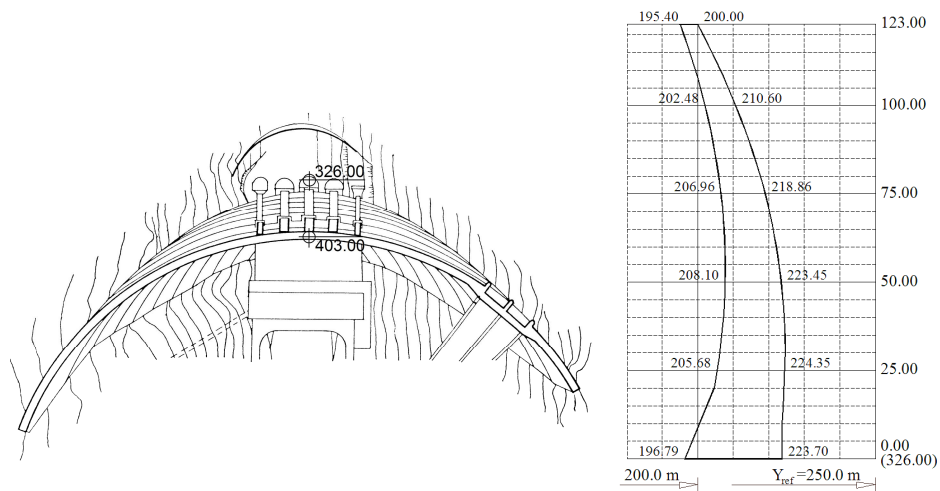


Figure 20. Plan of the dam body with land topology (left) and cross section through central cantilever (right) [29]

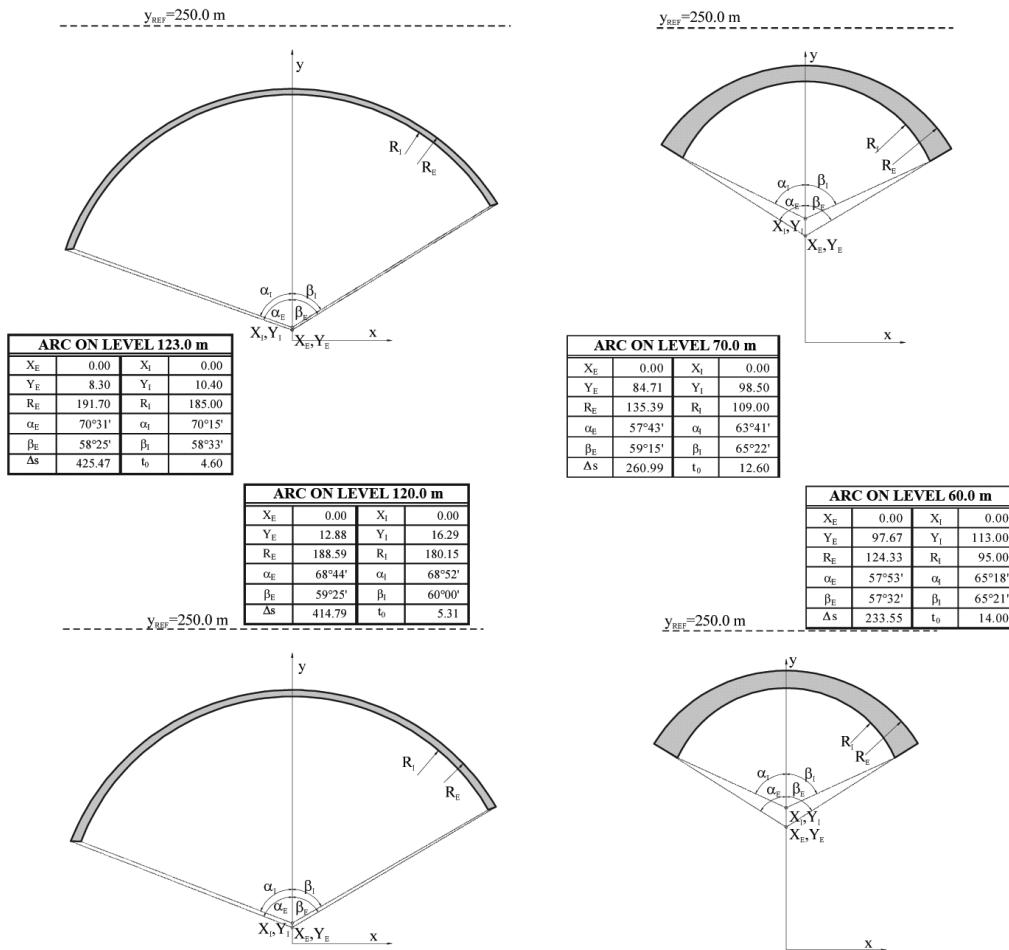


Figure 21. Geometry of some arch elements of the Gran arevo dam [29]

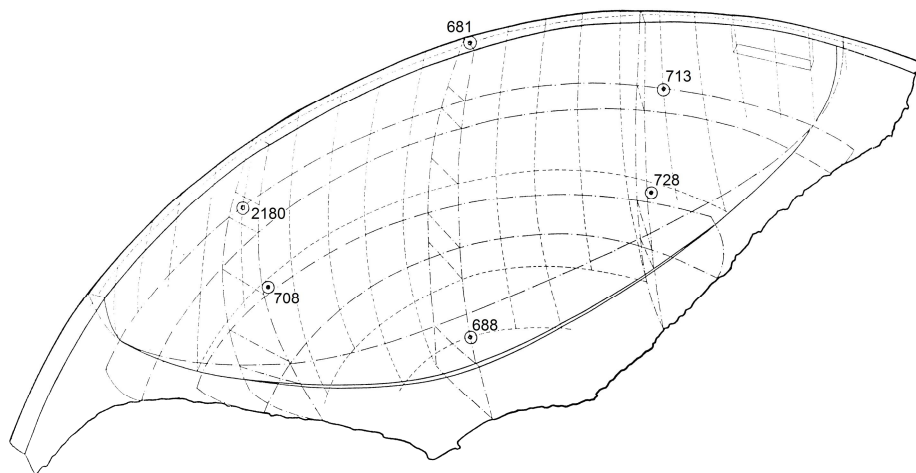


Figure 22. Positions of accelerographs in the Gran arevo dam body [29]

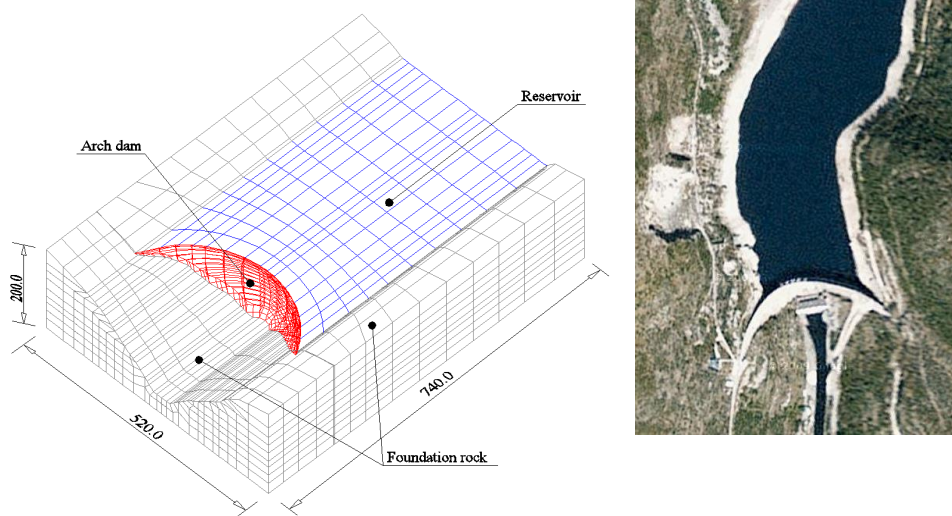


Figure 23. Finite element mesh of the Gran arevo dam. water. foundation rock interaction system . axonometric view and aerial view (Google map)

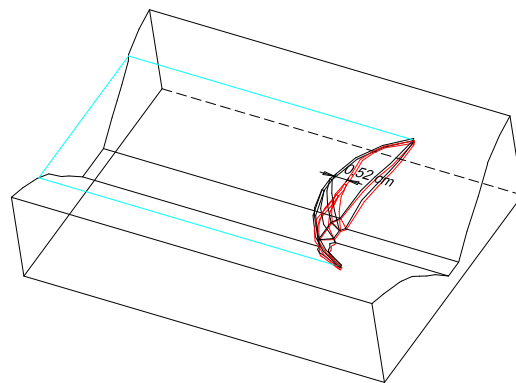


Figure 24. Displacement of the dam's self weight and hydrostatic pressure of water

The Institute of Earthquake Engineering and Engineering Seismology (IZIIS-Skopje, Macedonia) monitored the dam and performed several numerical simulations on different models, which were compared with results in situ [29]. All applied models included only the dam (structure), and water was treated as an additional mass on structure.

The complex model of the water-dam-foundation rock system is presented in Fig. 23. Material characteristics are given in Table 2. For the dam and foundation rock 27-node (brick) elements are used, as well as for the accumulation (fluid). For the simulation of connections between the foundation rock and the structure 18 nodes contact elements are used.

The dam is first analyzed for the self weight and hydrostatic pressure of accumulated water. The water level in the accumulation (reservoir) is at a relative elevation of 120.0 m (3.0 m below the crest). Displacements' field for this load is relatively small. The displacement in the crest of the dam is 0.52 cm in the horizontal direction (perpendicular to the crest) and 0.62 cm in the vertical direction. These results are in very good agreement with the results of the dam monitoring (0.58 cm in the horizontal direction and 0.68 cm in the vertical direction). Fig. 7 shows the displacement of the dam's self weight and hydrostatic pressure of water.

The behavior of coupled system dam-water-foundation rock was analyzed for the registered earthquake from 1986, [29, 30] . Fig. 25.

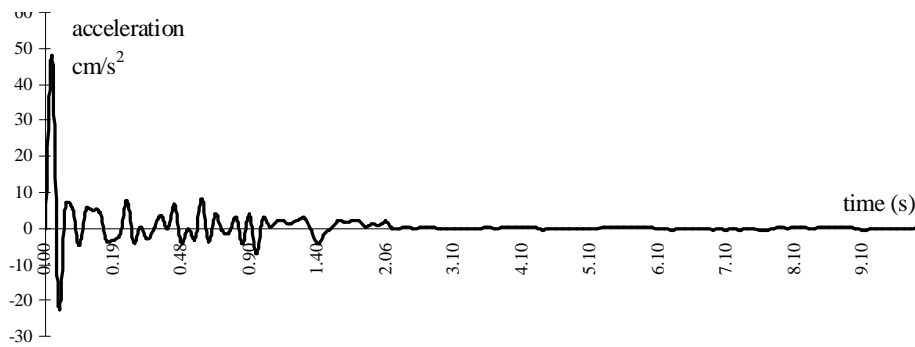


Figure 25. Registered earthquake in accelerograph 688 in Fig. 21

Fluid (water)	Structure (concrete dam)	Foundation rock
$\rho_f = 981 \text{ kg/m}^3$ $c = 1440.0 \text{ m/s}$	$E_c = 33000.0 \text{ MPa}$ $\nu_c = 0.15$ $\rho_c = 2400.0 \text{ kg/m}^3$ $f_{ck} = 25 \text{ MPa}$ ; $f_{ct} = 2.5 \text{ MPa}$ $\epsilon_t = 0.083$ ; $\epsilon_{t,max} = \epsilon_{s,max} = 1.7$	$E_r = 80 \text{ GN/m}^2$ $\nu_r = 0.2$ $\rho_r = 2620.0 \text{ kg/m}^3$ $f_{rk} = 12.0 \text{ MPa}$ ; $f_{rt} = 1.2 \text{ MPa}$

Table 2. Material characteristics of Gran arevo dam system

To determine the dynamic characteristic of the dam, analysis of the structure oscillation (modal analysis) was conducted [3, 7, 11]. The analysis was performed for the coupled system: dam, rock and water (full accumulation). The results of analysis, Fig. 26, are showing for the first four eigenvectors. It can be seen very good agreement with the results presented in the literature [31].

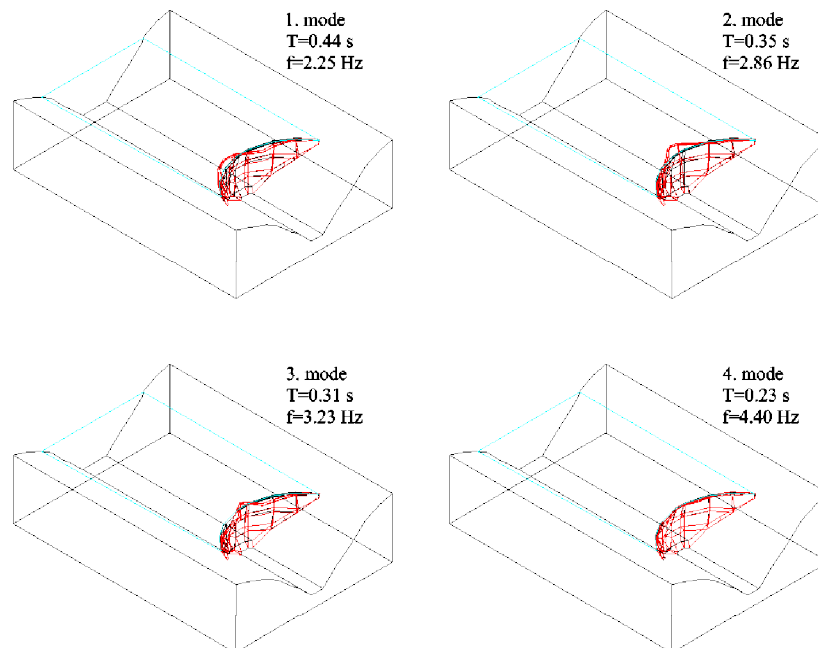


Figure 26. Oscillation periods, frequencies and eigenvectors for dam-accumulation system



Based on the calculated data, time step for dynamic analysis was adopted as  $\Delta t=0.002$  s, which represents approximately 1/200 of first period ( $T_1$ ), and also well approximate given accelerogram (Fig. 25). Time integration of equations of motion was performed by implicit method for water and construction.

Then, the registered accelerations on the bottom of the dam (accelerograph 688, Fig. 22) were taken as imposed accelerations of the foundation rock (excitation) along the canyon (perpendicular to the dam axis). The maximal registered imposed acceleration was  $47.8 \text{ cm/s}^2$ . The maximal registered acceleration on the dam was  $145.1 \text{ cm/s}^2$  (accelerograph 681, Fig. 22), and the maximal acceleration obtained through the numerical model was  $149.3 \text{ cm/s}^2$  (Fig. 27). Applied excitations cause hydrodynamic pressures that are always less than the hydrostatic pressure, so cavitation did not occur.

Some calculation results are presented in Figs. 27, 28 and 29. Fig. 27 presents accelerations of the Gran arevo dam crest in time, Fig. 28 presents displacement of the Gran arevo dam crest in time and Fig. 29 presents hydrodynamic pressures on the bottom of the Gran arevo dam in time. Other results can be found in [29, 30, 31].

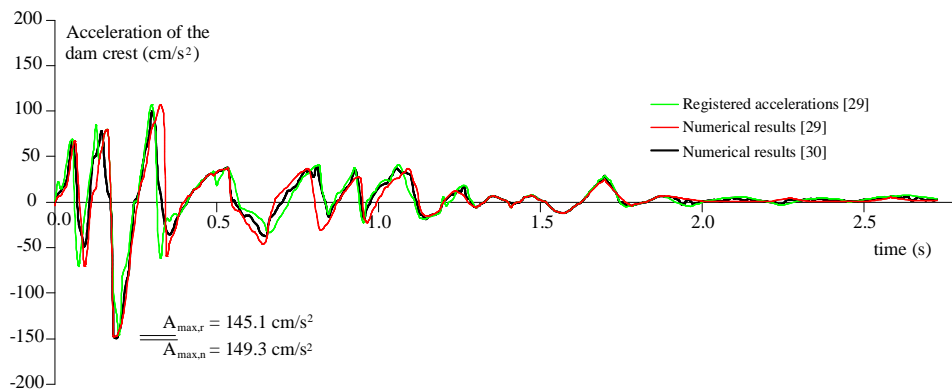


Figure 27. Accelerations of the Gran arevo dam crest

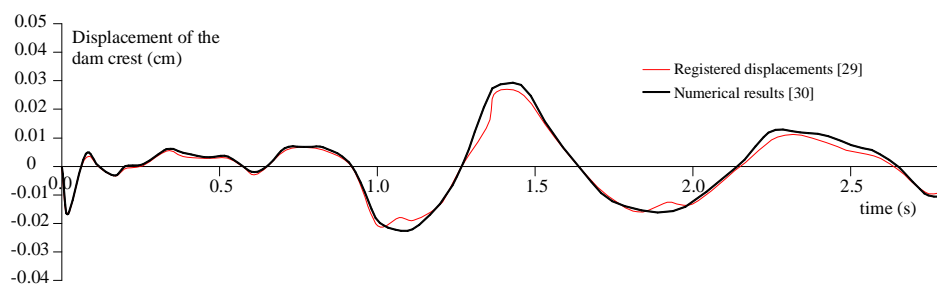


Figure 28. Displacement of the Gran arevo dam crest

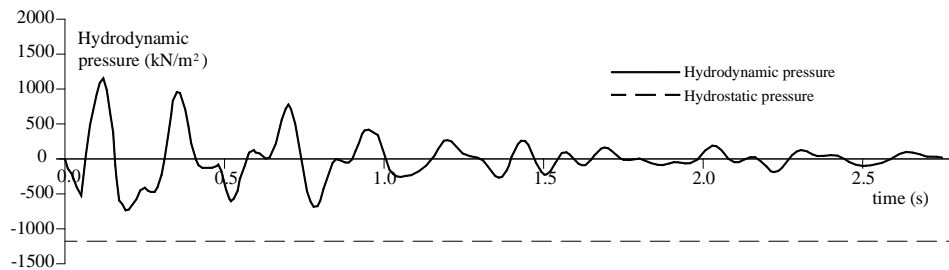


Figure 29. Hydrodynamic pressures on the bottom of the Gran arevo dam

### 3.3. Example 3- Underwater tank "Khazzan"

Khazzan (meaning: *To Store* in Arabic) was the name given to the tanks designed and built in late 1960s to store Dubai's Oil by Chicago Bridge and Iron Company. Dubai's Khazzans are unique in that they store Dubai's Oil under the Sea. Khazzan is a 500.000 barrel (80.000 m<sup>3</sup>) oil storage tank (Fig. 30). The 15.000 ton structure is 80 m in diameter on bottom and 8 m diameter on top, and about 82.0 m in height. Sea depth is about 70 m, so tank crest is 12 m under sea level. It has no bottom and operates on the water displacement principle. It is filled by placing oil in the tank above water where the additional weight of the oil on the water creates an imbalance in pressure. This force pressures the water out of the tank through the openings in the wall at the bottom.

Initial construction was in a shallow, dewatered basin. When the tank was sufficiently complete so that it could float as a single unit, using compressed air, the basin was flooded, and the tank, a bottomless hemisphere, was moved laterally into a deeper basin and seated on its floor by releasing the internal air pressure. The structure was then fully completed. Floated once again by filling the tank with compressed air, it was towed to the site and positioned by mooring lines, and the air was gradually released. It was allowed to slowly sink further and settle on the seafloor [34].

The geometrical characteristic of the model were taken from [32, 34, 35]. Fig. 31 shows the vertical section of the oil tank with the adjacent part of the surrounding sea.

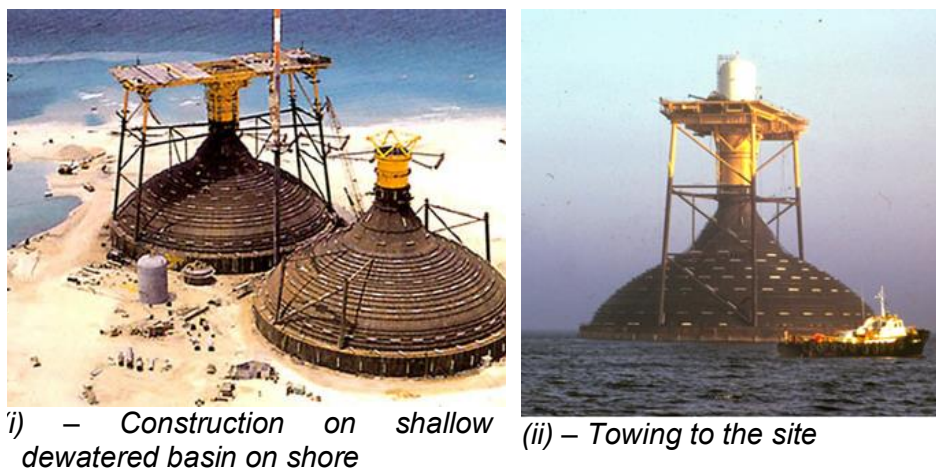


Figure 30. Oil-storage tank Khazzan [34, 35]



Fluid . sea water	Fluid . oil	Structure . steel (tank)
$\rho_f = 1000.0 \text{ kg/m}^3$ $c = 1430.0 \text{ m/s}$	$\rho_n = 900.0 \text{ kg/m}^3$ $c = 1300.0 \text{ m/s}$	$E = 210 \text{ GN/m}^2$ $\nu_t = 0.3$ $\rho_a = 78.5 \text{ kN/m}^3$

Table 3. Material characteristics of the Khazzan store tank

The sea-oil-tank system was modeled with the spatial 3D model, shown in Figs. 31 and 32. Spatial discretization of the liquid was done with 27-node 3D brick elements, and the structure with 9-node shell elements.

The harmonic ground acceleration with the period of 0.207 s (which is in accordance with the first period of the sea-oil-tank system), and amplitudes of 0.3 g for the horizontal and 0.2 g for the vertical acceleration component is accepted. The material characteristics are shown in Table 3. Implicit time integration ( $\Delta t=0.002$  s) and diagonal mass matrix were used.

Some results are shown in Figs. 33-36, and a detailed description of the model and results can be found in [32].

Fig. 33 shows the hydrodynamic water pressure for the horizontal seismic action in the specified points on the tank surface and Fig. 34 shows the horizontal displacements of the specified points of the tank for the horizontal seismic action. Fig. 35 shows the maximal displacements of the Kazzan oil-storage tank for the horizontal and the vertical seismic action.

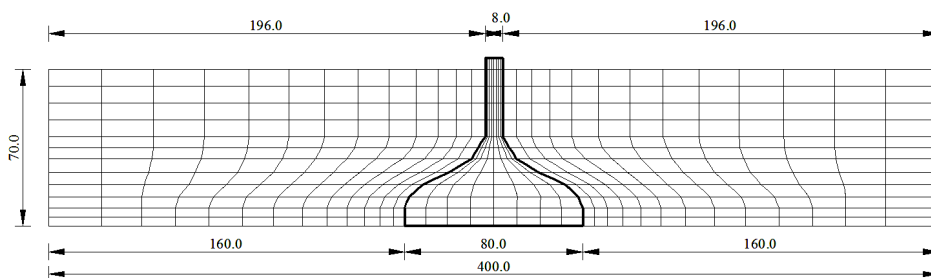


Figure 31. Spatial discretization of the Kazzan tank, the oil in the tank and the surrounding sea water . Longitudinal section of the finite element mesh (all dimensions in meters)

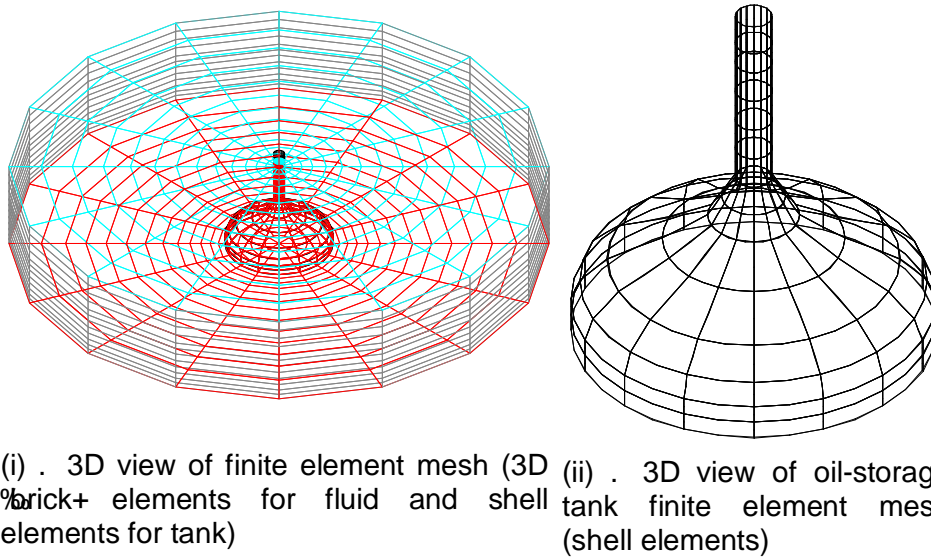


Figure 32. Spatial discretization of the Kazzan tank, the oil in the tank and the surrounding see water . axonometric view

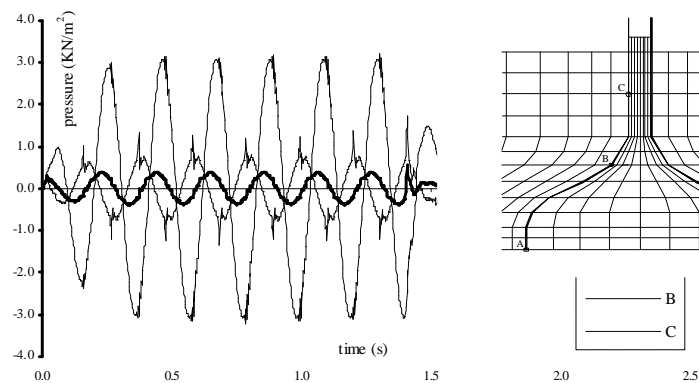


Figure 33. Hydrodynamic water pressure in the specified points on the surface of the Kazzan oil-storage tank for the horizontal seismic action

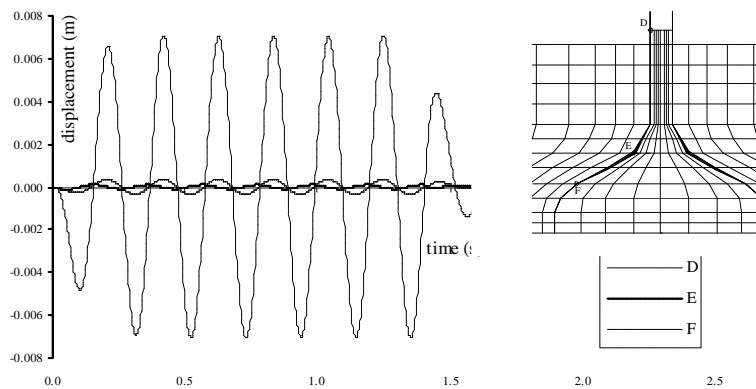


Figure 34. Horizontal displacements of the specified points of the Kazzan oil-storage tank for the horizontal seismic action

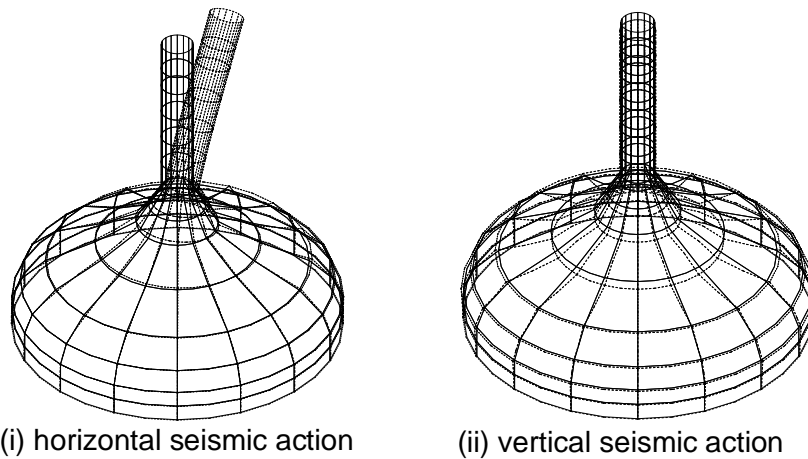
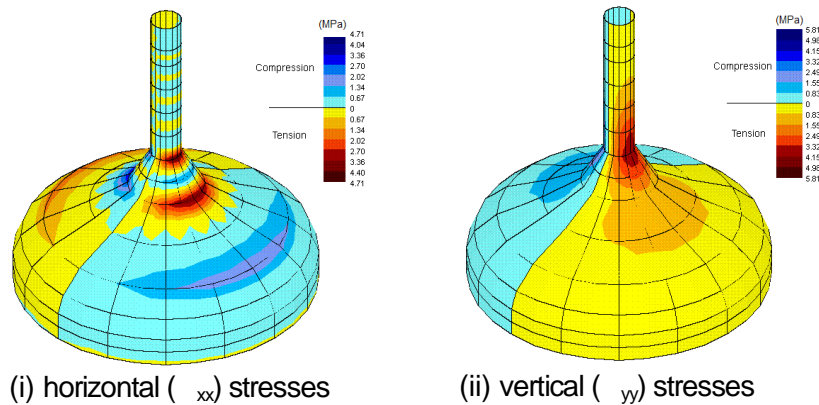


Figure 35. The Kazzan oil-storage tank maximal displacements

Figure 36. Maximum stresses of the Kazzan oil-storage tank in  $t = 0.73$  s, for the horizontal seismic action

### 3.4. Example 4- Underwater tunnel "Høgsfjord"

The seismic behavior of the planned (but not yet realized) underwater tunnel "Høgsfjord" in Norway was analyzed. The tunnel is about 1400 m long and 20 m immersed in the sea. It is connected to the sea-bed with cables every 200 m (axial distance) (Fig. 37).

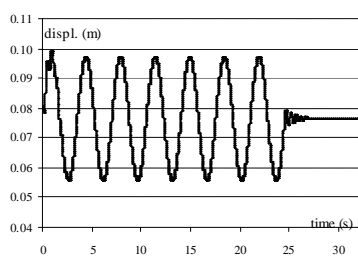
The tunnel has a circular cross-section with a 8.6 m inner diameter and 50-80 cm thick walls (Fig. 37). Intended construction material for the tunnel is prestressed concrete. Some other information about the planned structure can be found in [32, 36]. The material characteristics are shown in Table 4.



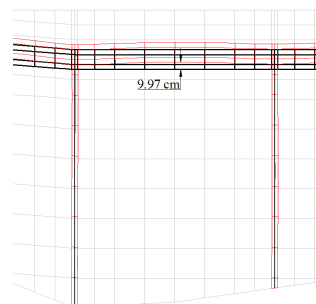


<b>CONCRETE</b>	Modulus of elasticity		Poisson's coefficient		Density		Compression strength					
	$E_c$ (GN/m <sup>2</sup> )		$\nu_c$		$\rho_c$ (KN/m <sup>3</sup> )		$F_{ck}$ (MN/m <sup>2</sup> )					
	36.0		0.2		25.0		40.0					
<b>STEEL</b>	<b>- REINFORCING STEEL -</b>											
	Modulus of elasticity		Poisson's coefficient		Density		Hardening modulus		Yielding strength		Ultimate strength	
	$E_s$ (GN/m <sup>2</sup> )		$\nu_s$		$\rho_s$ (KN/m <sup>3</sup> )		$H_s'$ (GN/m <sup>2</sup> )		$\sigma_{ys}$ (MN/m <sup>2</sup> )		$\sigma_{us}$ (MN/m <sup>2</sup> )	
	210.0		0.3		78.5		0.0		400.0		500.0	
	<b>- PRESSTRESSING STEEL -</b>											
	Modulus of elasticity		Poisson's coefficient		Density		Hardening modulus		Yielding strength		Ultimate strength	
	$E_{ps}$ (GN/m <sup>2</sup> )		$\nu_{ps}$		$\rho_{ps}$ (KN/m <sup>3</sup> )		$H_{ps}'$ (GN/m <sup>2</sup> )		$\sigma_{yps}$ (MN/m <sup>2</sup> )		$\sigma_{ups}$ (MN/m <sup>2</sup> )	
210.0		0.3		78.5		0.0		1570.0		1770.0		
<b>STEEL FOR TENDONS</b>	Modulus of elasticity		Poisson's coefficient		Density		Hardening modulus		Yielding strength		Ultimate strength	
	$E_B$ (GN/m <sup>2</sup> )		$\nu_b$		$\rho_a$ (KN/m <sup>3</sup> )		$H_s'$ (GN/m <sup>2</sup> )		$\sigma_y$ (MN/m <sup>2</sup> )		$\sigma_u$ (MN/m <sup>2</sup> )	
	210.0		0.3		78.5		0.0		1570.0		1770.0	
<b>SEA WATER</b>	Velocity of sound				Density of sea water							
	$c$ (m/s)				$\rho_w$ (KN/m <sup>3</sup> )							
	1500.0				10.5							

Table 4. Material characteristics of Høgsfjord+tunnel

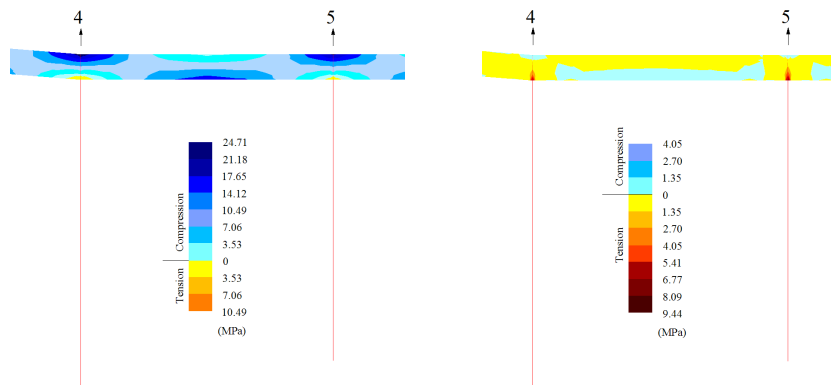


(i) Displacement of the point A of the tunnel in time



(ii) The maximal tunnel deflections

Figure 40. Displacements of Høgsfjord+tunnel, segment 4-5



(i) Maximal horizontal stresses ( $\sigma_{xx}$ ) (ii) Maximal vertical stresses ( $\sigma_{yy}$ )

Figure 41. Stresses of %Høgsfjord+tunnel, segment 4-5

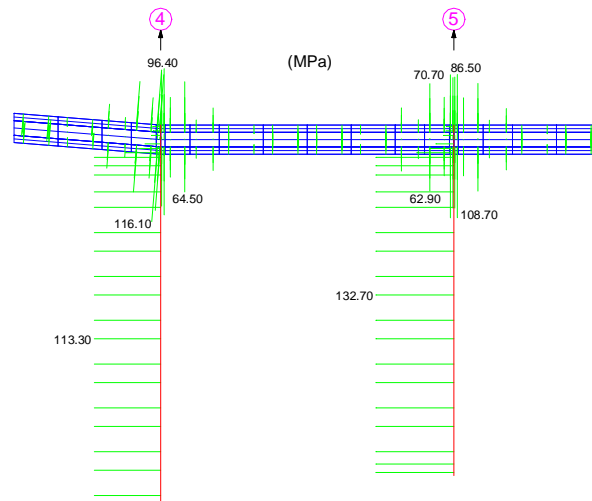


Figure 42. Stresses in reinforcement and cables, %Høgsfjord+tunnel, segment 4-5

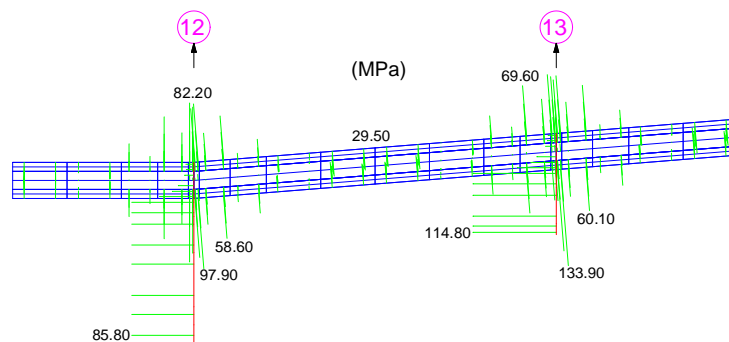


Fig. 43. Stresses in reinforcement and cables, %Høgsfjord+tunnel, segment 12-13



#### 4. CONCLUSION

The presented models for the dynamic (seismic) analysis of various types of structures that are in contact with fluid can simulate some of the most important non-linear effects. The models are simple, reliable and can be used in a wide range of practical problems. Shown examples illustrate some of the possibilities of the models and the developed computer programs (software) for various types of engineering structures.

#### REFERENCES

1. Bathe K.J. and Hahn W.F.: On transient analysis of fluid-structure system, *Computers and Structures*, 10, 383-391, (1979)
2. Owen D.R.J., Hinton E.: *Finite Elements in Plasticity*, Pineridge Press, Swansea, UK, (1980)
3. Paul Dilip K.: Efficient dynamic solutions for single and coupled multiple field problems, PhD Thesis, University College of Swansea, (1982)
4. Wilson E.L., Yuan M., Dickens J.M.: Dynamic analysis by direct superposition of Ritz vectors, *Earthquake Eng. & Struc. Dyn.*, 10, 813-832, (1982)
5. Radni J., Damjani F. B., Jovi V.: Hydrodynamic pressures on rigid structures, *Proc. European Conf. on Earth. Eng., Portugal*, (1986)
6. Radni J.: "Fluid-structure interaction with cavitation effect", *Gra evinar*, 7, 269-275, (1987) (in Croatian)
7. Damjani F.B., Radni J.: Seismic Analysis of Fluid-Structure Interaction Including Cavitation, *Proc. Int. Conf. on Computer Modelling in Ocean Engineering*, Balkema, Rotterdam, 523-530, (1988)
8. Yuan M., Chen P., Xiong S., Li Y., Wilson E.L.: The WYD method in large eigenvalue problems, *Eng. Comp.*, 6, 49-57, (1989)
9. Mihanovi A., Schönauer M.: Modified WYD method in large dynamics eigen problems+, *proc. 19. simp. of Yugoslav society of mechanics*, Bled, (1989) (in Croatian)
10. Huang H.C.: *Static and Dynamic Analyses of Plates and Shells*, Springer-Verlag, Heilderberg, (1989)
11. Bangash M. J. H.: *Concrete and concrete structures: Numerical modelling and applications*, Elsevier Applied Science, New York, (1989)
12. Radni J., Dezkovi N.: Numerical model for dynamic analysis of RC structures including the strain rate effects, *Proc. 2nd Int. Conf. on Comp. Plasticity*, Barcelona, 65-71, Pineridge Press, Swansea, (1989)
13. Radni J.: Modelling of strain rate effects in dynamic analysis of R/C structures, *Engineering Mod.*, 3, No. 1-2, 13-20, (1990)
14. Phillips D. V.: Numerical modelling of brittle materials; concrete and reinforced concrete, *Lecture Notes on Nonlinear Engineering Computation*, TEMPUS-ACEM, Ljubljana, C/1-78, (1992)
15. Hofstetter G. and Mang H. A.: *Computational mechanics of reinforced concrete structures*, Vieweg&Sohn, Weisbaden, Germany, (1995)
16. Lofti V.: Application of pseudo-symmetric technique in dynamic analysis of concrete gravity dams, *Advances in Fluid Mechanics*, 36, 207-216, (2003)
17. Lofti V.: Seismic analysis of concrete gravity dams by decoupled modal approach in time domain, *Electronic Journal of Structural Engineering*, 3, 2003.



18. Sekulovi M., Mrdak R., Pejovi R., Mijuzkovi O.: Analysis of seismic response of high arch dam on basis of energy balance, 13<sup>th</sup> World Conference on Earthquake Engineering, Canada, Vancouver, (2004)
19. Küçükarslan S., Co kun S.B., Ta kin B.: Transient analysis of dam-reservoir interaction including the reservoir bottom effects, *Journal of Fluids and Structures*, 20 (8), 1073-1084, (2005)
20. Pin F. D., Idelsohn S., Oñate E., Aubry R.: The ALE/Lagrangian Particle Finite Element Method: A new approach to computation of free-surface flows and fluid-object interactions, *Computers and Fluids*, 36 (1), 27-38, (2007)
21. Ortega E., Oñate E., Idelsohn S.: An improved finite point method for three dimensional potential flows, *Computational Mechanics*, 40 (6), 949-963, (2007)
22. Harapin A., Radni J., ubela D.: Numerical model for composite structures with experimental confirmation, *Materialwissenschaft und Werkstofftechnik*, 39 (2), 143-156, (2008)
23. Harapin A., Radni J., Brzovi D.: WYD method for an eigen solution of coupled problems, *Int. Jnl. of Multiphysics*, 3 (2), 167-176, (2009)
24. Gali M., Marovi P., Nikoli ž., Harapin A.: Numerical modelling of tension influences in 3D reinforced concrete structures, *Proceedings of the 10<sup>th</sup> International Conference on Computational Plasticity*, Onate E.; Owen R.; Suarez B., Barcelona, CIMNE, 539/1-539/4 (2009)
25. Krishna J., Chandrasekaran A. R., Saini S. S.: Analysis of Koyna accelerogram of December 11, 1967., *Bulletin of Seismological Society of America*, 59, 4, 1719-1731, (1969)
26. Chopra A. K., Chakrabarti P.: The Koyna earthquake and the damage of Koyna dam, *Bulletin of Seismological Society of America*, 63, 381-397, (1973)
27. %esperienze Statiche su Modello Della Diga di Grancarevo+, I.S.M.E.S. Istituto Sperimentale Modelli e Strutture, Bergamo, Settembre 1960., pratica no. 271 (in Italian)
28. %Sulla StabilitaqDella Roccia di Fondazione Della Diga di Grancarevo Verificata Anche a Mezzo Modello Geomeccanico+, I.S.M.E.S. Istituto Sperimentale Modelli e Strutture, Bergamo, Settembre 1963. (in Italian)
29. Bi kovski V., Bojad0iev M.: Studies of static and seismic analysis of Gran arevo dam, The Institute of Earthquake Engineering and Engineering Seismology University "Ss. Cyril and Methodius" (IZIIS) Skopje, Macedonia, Report IZIIS 88-30, (1988) (in Serbian)
30. Harapin A.: Numerical model of fluid-structure dynamic interaction, PhD Thesis, University of Split, Faculty of civil engineering, (2000)
31. Pejovi R., Mrdak R., živaljevi R., Mijuzkovi O.: An analysis of seismic resistance of the Gran arevo concrete dam, *Gra evinar*, 58, 447-453, (2006) (in Croatian)
32. %unji G.: Numerical model of seismic response of submerged structures, MD Thesis,, University of Split, Faculty of civil engineering and architecture, (2003) (in Croatian)
33. [www.indianetzone.com/34/koyna\\_dam\\_maharashtra.htm](http://www.indianetzone.com/34/koyna_dam_maharashtra.htm)
34. [www.dubaiasitusedtobe.com](http://www.dubaiasitusedtobe.com)
35. [www.coastal.udel.edu](http://www.coastal.udel.edu)
36. [www.ntnu.no/gemini/1998-01E/36.html](http://www.ntnu.no/gemini/1998-01E/36.html)